
Article:
Worden, K. orcid.org/0000-0002-1035-238X, Spencer, A.B., Packo, P. et al. (3 more authors) (2018) Acoustic emission source characterisation using evolutionary optimisation. Strain, 54 (4). e12272. ISSN 0039-2103

https://doi.org/10.1111/str.12272

Acoustic Emission Source Characterisaton using Evolutionary Optimisation

K. Worden[a 1], **A.B. Spencer**[a] **P. Packo**[b], **W.J. Staszewski**[b], **T. Uhl**[b] and **S.G. Pierce**[c]

[a]Dynamics Research Group, Department of Mechanical Engineering, University of Sheffield, Mappin Street, Sheffield S1 3JD, UK
[b]AGH University of Science & Technology, Department of Robotics & Mechatronics, PL-30059 Krakow, Poland
[c]Centre for Ultrasonic Engineering, Department of Electronic & Electrical Engineering, University of Strathclyde, Glasgow G1 1XW, UK

Abstract

When a crack initiates and grows in a metal or composite structure, for example due to high cycle fatigue, the crack propagation gives rise to acoustic emissions (AE) – ultrasonic waves travelling through the structure. Because the presence and rate of growth of any cracks are important pieces of information about the condition/health of the structure, the monitoring of AE activity using sensors mounted on its surface is a potentially useful technique of Structural Health Monitoring (SHM). In tests, acoustic emissions are often simulated by breaking a pencil lead against the surface of the structure in a standardised way (a 'Hsu-Nielsen' source), but the forces that this imparts are not well understood at present. The current paper proposes a new evolutionary optimisation-based approach to source characterisation. The principle is to introduce a parametrised representation of a general source and then identify the parameters that allow the source to best match responses measured elsewhere on the structure. The predicted responses are modelled using a Local Interaction Simulation Approach (LISA) algorithm to simulate the propagation of the ultrasonic waves. The approach is validated here using experiments on AE propagation in thin plate-like structures, where the ultrasound propagates as Lamb waves. Three separate case studies are proposed here. In the first case, an idealised point source is simulated using laser-generated ultrasound and the optimisation algorithm uses a two-dimensional (2D) LISA model. A Differential Evolution (DE) optimisation scheme is used to find the optimal profile of forcing to match the simulation with experiment. In the second case, the 2D LISA approach is used to characterise the forces associated with standard pencil lead breaks. The final study addresses the full three-dimensional (3D) wave propagation. Because of the computational expense of the latter calculation, the LISA algorithm is implemented using a CUDA graphics card computer system.

Key words: Acoustic emission (AE); Source characerisation; Local Interaction Simulation Approach (LISA); Differential Evolution; CUDA.

1 Introduction

The subject of Structural Health Monitoring (SHM) has been the focus of considerable activity in recent years and offers a potentially key technology for the optimisation of design and maintenance in the contexts of structural design and safety. One of the more promising SHM technologies for detection and localisation of incipient or small damage is based on guided-wave ultrasonics, where diagnostic information is provided by interpreting the passage of high-frequency waves through the structure as they interact with local damage e.g. when reflected or scattered from fatigue cracks. In most cases, guided waves result as the geometry of the structure will cause it to act (act least locally) as a waveguide; in particular, the presence of thin plate-like elements will cause any ultrasound to propagate as Lamb waves within them [1]. The physics of guided-wave propagation can be quite complex as the waves will be modal and dispersive [1, 2]. In terms of guided-wave SHM, both *active* and *passive* approaches have been developed. In the former case, waves are deliberately initiated in the structure using some appropriate form of actuation [3, 4]; the response wave profiles at various points on the structure are then sensed and can be used to derive diagnostic information. In the passive approach, the guided-waves

[1]Corresponding Author: k.worden@sheffield.ac.uk

of interest are generated naturally within the structural as a result of its loading and operating conditions. The most well known passive approach to ultrasonic SHM is that based on *Acoustic Emissions* (AE). These are small bursts of ultrasound generated by various mechanisms within a structure which propagate and can be measured by surface-mounted sensors. The interest of AE for SHM purposes is provided by the fact that the growth of damage (e.g. fatigue cracks in metals or delaminations in composites) is among the mechanisms that generate AE [5]. In the context of passive guided-wave SHM, based on AE, it may prove very useful to characterise the nature of the source. In particular for SHM, it is very important to distinguish burst AE due to crack propagation from any other potential sources of confusion.

Although powerful data-based approaches to AE-based SHM have been developed (a sample from the current authors and their colleagues is [6, 7, 8]; also see the references therein), it will clearly be advantageous to have some means of understanding and simulating the underlying physics of the source generation and wave propagation in the structure. The information available from such simulations can be used in many ways including guiding the deployment of sensors or choosing appropriate features for interpretation as damage indicators. In the recent past, there has been considerable work carried out on the computational simulation of guided-wave propagation (a fairly recent literature survey is available as [9]), and the Local Interaction Simulation Approach (LISA) has emerged as an attractive method due to its conceptual simplicity, ease of implementation and numerical efficiency [10, 11, 12, 13, 14]. One of the motivations for the current programme of work, was the need to experimentally validate the LISA simulations in order to provide confidence in the formulation and also in the numerical implementation. Leaving aside the issue of wave propagation for the moment, it is fair to say that the mechanisms of source generation and thus of characterisation are not completely understood in the context of AE. This observation leads to the other motivation for this paper, which is to develop a means of characterisation based on an optimisation approach. The term *characterisation* is being used here in preference to the term *identification*. The idea here will be to specify some imposed force or displacement profile which, when used in a model, correctly reproduces real AE burst responses at some measurement points distant from the point of application.

Before proceeding, it is important to consider what has already been achieved and reported in the literature. The problem of source characterisation has been considered for many years. However, when one searches for references on source *characterisation* or source *identification*, one finds a great deal of the work (particularly recently) is actually concerned with *classification*; i.e. the problem of assigning a label to the source indicating the mechanism using pattern recognition or machine learning methods. Such references will not be cited here, beyond identifying a couple of examples where the reader can see the general idea [15, 16]. The problem of interest here is actually to infer the time-dependent source function; this can be approached in various ways: experimentally, by using physics-based models, and by using data-based models. It is not the intention of this paper to give a complete literature survey; the ambition here is simply to give examples of how the various approaches have been pursued with some success.

In terms of experimental approaches to the problem, one fascinating early study is [17]; there the authors treat the problem as a deconvolution problem and address it directly in the time domain. They consider a number of different source mechanisms, including: breaking a glass capillary, breaking a pencil lead, dropping a steel ball and inducing brittle fracture in a glass plate by impact of a diamond indenter. Some qualitative observations are made about the results. The careful study [18], looks at the deconvolution approach and makes a more careful mathematical analysis of the elements of the inverse problem. In particular, an attempt is made to mathematically model a source representing the creation and growth of an infinitesimal planar elastic microcrack – a very idealised problem. Another interesting early study is provided by [19], which considers fibre fractures in tungsten/copper composites; the paper considers the elements of the inverse problem, including the need to identify the transfer function of the transducer. The problem is summed-up nicely in the statements in [20]: 'However, it is difficult to deduce the form of the elastic wave leaving the source once the energy has been converted into surface and plate waves and hence to characterise the source event' and 'Full deterministic characterisation is, however, always likely to be limited in the applications for which it can be used and to require expensive computing facilities'. However, one notes that, in 1987, it was difficult to anticipate quite how powerful relatively inexpensive computers would become. Jumping forward in time a little, one finds [21], which is of particular interest here as it treats the case of laser-generated ultrasound, including the different physical mechanisms by which the sound is generated. In

general, it appears that source characterisation is most often formulated as an inverse problem, with more modern approaches based on moment tensors and their inversion [22]. The current paper presents a different view based on optimisation, where the only calculations carried out are forward simulations from source to response.

The results from an optimisation approach will only be as sensible as the results from the forward simulations on which it depends. The approach presented here has adopted the LISA algorithm; however, the literature shows that other physics-based models would prove equally effective; particularly with recent increases in computational power. The numerical approaches are capable of not only capturing wave propagation in various media, but also of representing the physics of various AE source mechanisms. The paper by Prosser *et al* [23] is of interest because it proposed both a semi-analytical approach based on Mindlin plate theory and a dynamic Finite Element (FE) approach. In both cases, the AE source of interest was a step-function load applied as a point source on a plate surface. The paper considered propagation in both isotropic (metallic) and anisotropic (composite) plates. The paper did not make any detailed comparisons with experiment, but showed that the Mindlin theory results agreed well with those from FE. The main advantage of the Mindlin plate model was in the speed of computation, compared to FE, while the FE model proved far more versatile in terms of geometry and source function. Finite models of the response to more realistic sources, in particular those from the fracture of glass capillaries and pencil leads. Capillaries were considered in [24], which looked at the FE modelling of a glass capillary fracture on a large steel block, and the results from the model were compared with experiment. A 'cosine-bell' temporal profile was used for the source. The model results were shown to be similar to the experimental measurements in terms of a number of key features, including arrival times of the bulk longitudinal waves, the shear waves and the Rayleigh waves. It was shown that the response predictions were sensitive to the shape parameters of the source, which at the time could not be measured. The paper also considered the effect of transducer bandwidth on response predictions. The paper [25] considered the FE modelling of pencil lead breaks (Hsu-Nielsen sources); a multi-scale model was presented with dynamic boundary conditions. The work was validated against a series of experiments where leads were broken against a block; different lengths of the lead and angle against the block were considered. A contact model was used for the FE, with a simplified fracture model; the results agreed very well with the experimental measurements when validated via measured rupture forces. The source function modelled was then compared to some of the analytical forms used in the literature up to that point, and the best agreement was found with the cosine-bell source. Looking at complex media, the paper [26] considered FE modelling of Lamb wave propagation from AE sources in anisotropic plates; hybrid plates typical of composite pressure vessels were investigated. The waves in the layered media from AE sources were shown to propagate as Lamb waves together with waves in the individual layers. The results were validated experimentally using pencil-lead breaks on an aluminium plate where the responses were measured using a laser vibrometer. In the FE model, the source was simulated using a linear ramp function as proposed in [27]; the response predictions of the model showed good agreement with experimental measurements taken 100mm from the source. The FE modelling approach was also extended to crack sources in [28]. The crack was modelled using a cohesive zone approach and the overall multi-scale multi-physics approach included the modelling of the piezo-electric transduction and acquisition electronics. Interestingly, their model did not require the specification of a force-time curve as a source function. The AE signals from the simulated crack sources were validated against the results of micro-mechanical experiments. The paper by [29] also considers the problem of modelling AE generation and propagation from cracks, but is closer in spirit to the current paper, because it incorporates a data-based element to the problem of source identification. In terms of the source, full field data from Digital Image Correlation are used to construction a traction-separation law, and to establish damage initiation parameters; for propagation, a 3D FE simulation was carried out based on a cohesive zone model, similarly to [28]. Experimental calibration/validation was carried out against data obtained from a compact tension specimen. The FE analysis was also carried out using the ABAQUS XFEM formulation to model crack onset and growth, with the CZM and XFEM predictions showing fairly good agreement.

In order to demonstrate and validate the optimisation-based source characterisation algorithm proposed here, the results of three case studies will be presented, in growing order of complexity. In each case, an acoustic source will be characterised based on data obtained in an experimental

test campaign. For the first case study, it was considered important to simplify or idealise the conditions of wave actuation, propagation and sensing as far as possible. In order to realise point-like actuation and sensing (in order to eliminate the dynamics of finite aperture sensors and actuators), laser actuation and sensing were used. Furthermore, in order to make the modelling of the wave propagation as simple as possible, a two-dimensional (2D) implementation of the LISA algorithm was applied. Once the characterisation approach was verified and validated in the idealised case, the second case study moved to a more practical problem. In experimental studies of AE, specimen bursts are often generated by breaking a pencil lead on the surface of the structure of interest; this type of source (a so-called Hsu-Nielsen source [30]) is commonly used for AE sensor calibration due to its comparatively repeatable nature. The second case study here will aim to characterise Hsu-Nielsen (HN) sources from experimentally-acquired data; as before, the 2D implementation of LISA will be used. The final case study looks at HN sources again, but this time makes use of a full three-dimensional (3D) LISA model. Initial attempts at the full 3D version of the approach proved almost impossible, due to the computational cost of the wave modelling needed for each objective function evaluation for the optimisation algorithm; this problem was solved by implementing the 3D LISA algorithm on a graphics-card-based computing engine – a CUDA system [31, 32, 33].

The layout of the paper is as follows: the next section describes the experimental campaign which generated the case study data. Section Three describes the main elements used in the methodology: the LISA algorithm used for simulation and the DE algorithm for optimisation. Sections Four, Five and Six describe the results from the case studies, in increasing order of complexity and the paper then finishes with discussion and conclusions.

2 Experimental Setup and Data Capture

The experimental methodology evolved considerably throughout the programme of testing. The original motivation for the programme was simply to provide wave response data that could be used to validate the LISA algorithm. The initial plan was to use piezoelectric transducers for both actuation and sensing. It was also assumed that the 2D implementation of LISA would be sufficient, as the plate was sufficiently wide that a clear time window for response could be obtained that did not contain any reflections from the side edge of the plate. The 2D implementation of LISA implicitly assumes that the plate has infinite width (the plate dimension perpendicular to the direction of wave propagation). Another assumption of the 2D algorithm, is that the wave propagates as a plane wave with the wavefront extending infinitely in the width direction; this latter assumption was more of a concern than the finite plate width, as the actuators used in the experiment could only launch a wave with a circular wavefront.

A problem immediately arose with the use of the piezoelectric transducers. While the voltage applied to the actuator and measured at the sensor could be specified and acquired accurately, it was clear that this was a long way from knowing the actual strains/displacements at either of the locations. The piezoelectric discs in their housings are complex dynamic systems themselves, which exhibit resonances and unequal sensitivity at different frequencies, and it was considered beyond the scope of the simulation at that stage to attempt to include the internal characteristics of the sensor and actuator in the LISA model. Furthermore, the precise spatial characteristics of the actuation or sensing across the diameter of the discs, or the relative sensitivity to in-plane and out-of-plane displacement exhibited by the sensor were unknown.

In order to eliminate one of the unknowns, it was decided to use a laser vibrometer to measure the out-of-plane displacement at the responses point; this gave a good approximation to a point sensor and effectively removed the spatial, directional and frequency-dependent uncertainty on the sensing side. However, the question of point actuation remained to be solved. One solution which presented itself, was to also use a laser to generate the source event, but using a Q-switched laser to actuate with a high-power pulse on the surface of the plate. This gave point actuation as required and also allowed very repeatable measurements; the response waveforms were measured by an Accelent oscilloscope triggered by a photodiode placed near the focal point of the actuation on the plate. Unfortunately another problem immediately arose. Using a high-power focussed laser concentrates the force onto a point spatially (on the scale of interest here); however, although the pulse itself has only a duration of a few nanoseconds (an interval much smaller than the anticipated time step of the LISA simulation), its effect in the time domain cannot be treated as instantaneous. The force on the plate surface imparted by the laser pulse is

caused by a combination of the explosive force of ablation at the surface of the aluminium and the rapid expansion and contraction of the metal due to heating and subsequent cooling.

In order to overcome the problem raised by the unknown temporal nature of the laser actuation, it was decided to simultaneously estimate the form of the source function and the corresponding wave responses in the plate. An optimisation procedure seemed to be an appropriate means of accomplishing this, so that the source function giving best agreement with the measured response could be obtained. The possibility thus arose that, as well as providing experimental validation for the LISA prediction of wave propagation, the approach could also provide a means of source characterisation which would prove useful in other contexts e.g. acoustic emission source characterisation, and a further sequence of tests was planned in order to investigate the characterisation of acoustic events from Hsu-Nielsen sources (pencil-lead breaks).

The first experimental configuration with laser actuation and sensing is shown in Figure 1. The plate used was 3mm thick Aluminium. The laser actuation presented a number of practical problems. One major issue was safety; due to the high power of the actuation laser, all tests were carried out in a closed room, with those present wearing blackout glasses during the laser activation. Another slight problem was caused by the configuration of the actuation laser, which did not allow the sensing laser to be focussed close to the point of actuation, so in the initial sequence of tests the response waveforms were recorded at distances of 6.3cm, 7.3cm and 8.3cm from the actuation point.

Figure 1: Experiment for data capture. The actuation laser is shown to the left of the aluminium plate and the laser vibrometer used for sensing is shown on the tripod on the right.

The later experiments with the Hsu-Nielsen sources used essentially the same setup as in Figure 1; the main difference being that actuation was from pencil-lead breaks on the surface of the plate. A standard 0.7mm extensible-lead pencil was used with 2H leads. Further details of the data acquired will be presented later in the results sections. For now, a brief summary of the computational methodology for source characterisation will be given.

3 Methodology

3.1 LISA: Implementation in Two Dimensions

The Local Interaction Simulation Approach (LISA) is a wave propagation simulation technique that was proposed in [10]. The algorithm is based on a discrete difference approach and has the benefits of conceptual simplicity and implementation speed. By using a *Sharp Interface*

Model to account for boundaries between materials, it can be used to model waves travelling through a heterogeneous material of arbitrary complexity. The LISA algorithm can model wave propagation in one [10], two [11] or three [12] dimensions; however, as one might expect, the complexity of the algorithm increases with dimension. The LISA algorithm was first investigated for SHM purposes, through the EU DAMASCOS project [34], and initially followed-up in [13, 14].

For the LISA approach, the structure under investigation is discretised into cells, where the material properties of the structure may differ between cells but are considered to be constant within each cell. The wave propagation within the structure is also discretised in time. The algorithm is a thus a powerful numerical technique for simulating wave propagation in heterogeneous media, where an analytical wave propagation solution is usually too complex. The algorithm is derived from the general elastodynamic wave equation [35],

$$\frac{\partial}{\partial x_l}\left(S_{klmn}\frac{\partial w_m}{\partial x_n}\right) = \rho\frac{\partial^2 w_k}{\partial t^2} \qquad (k,l,m,n = 1,3) \tag{1}$$

where S_{klmn} is the stiffness tensor, ρ is the material density and $\underline{w}$ is the particle displacement vector (w_1, w_2, w_3) corresponding to the standard Cartesian coordinates $\underline{x} = (x_1, x_2, x_3) = (x, y, z)$. Equation (1) is simplified in the two-dimensional (2D) case [11], and is implemented in a discrete difference form for LISA. In simple terms, the current particle displacement at each point on a discrete rectilinear mesh is given as a superposition of the previous values at that point and also values on neighbouring points in the mesh. The detailed derivation can be found in [11], although one should be aware that a number of small errors are present in the formulae within that paper; for ease of reference, these have been corrected in [36]. The two equations for the 2D particle displacements (w_1, w_3), rely solely on known material properties (the density and Lamé constants) for each cell and arbitrary discretisation steps, both spatial and temporal. In the current paper, because the plate material is homogeneous, the properties are held constant throughout the mesh. A LISA software package with a graphical user interface was initially created at the University of Sheffield using Java, and was used for 2D simulations here. As discussed later, the assumption that 2D modelling was appropriate may not be justified in some important respects; however, in terms of the initial development of the methodology here, it was considered to be a reasonable first approximation.

The simulations here made good use of lessons learned from a previous LISA simulation problem [37]. As part of that work, a benchmarking exercise was carried out in order to investigate issues like optimal setting of LISA cell size and time step. In fact, the cell size and time step are related by a stability condition specified in the original LISA papers [10, 11]; this is,

$$\frac{v\tau}{\epsilon} < 1 \tag{2}$$

where v represents the longitudinal velocity of sound in the medium or interest, τ is the timestep and ϵ the cell size. The paper [37] investigated the cell density needed in order to accurately represent the Lamb wave dispersion curves in an Aluminium plate. The conclusion reached was that the cell density needed in order to accurately represent dispersion characteristics for both S_0 and A_0 Lamb wave modes was 8 cells/mm. This means that 24 cells are needed across the thickness of the 3mm plate studied in this paper. Like many finite difference or finite element schemes, the computational effort required for LISA does not scale well with cell size. Because of the stability condition (2), halving the cell size also means halving the time step. It was also observed in [37] that, while 2D LISA calculations could be completed in minutes, 3D calculations required hours (precise timing are meaningless, given the developments in computer hardware since [37] appeared). The study [37] also compared the LISA results with those from a commercial modelling package and found better performance from the LISA algorithm in terms of both accuracy and speed.

3.2 LISA: Implementation in Three Dimensions

As mentioned earlier, there was some concern about out one of the assumptions of the 2D LISA implementation i.e. that the wavefront was a plane wave. Both of the sources investigated in this paper were point sources that generated a circular wavefront. Among the problems likely to be caused by the assumption, was the fact that energy would spread differently across the growing wavefront and that dissipation of energy with distance would be incorrectly represented. At the

time of the experiments, this problem appeared insoluble, as 3D simulations with LISA took far too long for implementation in an optimisation framework. Fortunately, a solution came along in the form of CUDA, which is a parallel processing computational architecture based on graphics cards as the numerical 'workhorses'.

When the 3D LISA algorithm [12] was implemented in the CUDA graphics card system [31, 32], initial results showed a factor of approximately 300 speed-up in the required 3D LISA calculations. The calculations were reduced from hours to minutes and it became feasible to use the 3D approach in an optimisation. A detailed benchmarking exercise on 3D LISA simulations can be found in [33].

3.3 Optimisation: Differential Evolution

As discussed earlier, the approach taken here to source characterisation is one of optimisation. The basic idea is to specify the 'source function' in LISA by a parametric model and to optimise the parameters in order to match the LISA predictions to a response measurement taken on the plate. The parametric form for the source function was chosen to be a sum of Gaussians,

$$s(t) = \sum_{i=1}^{N} a_i \exp\left[-5\left(\frac{t-\tau_i}{\tau_i}\right)^2\right] \tag{3}$$

where the parameters a_i are determined by the optimisation. The factor of 5 and the durations τ_i were fixed prior to the optimisation at values suggested by trial and error, in order to keep the number of parameters for optimisation under control. A few short optimisation runs were carried out in order to find the range of τ_i values which were able to influence the result; the τ_i were then placed across this range. Initial experimentation also showed that 10-15 Gaussians were sufficient to represent the source event. (The sum of Gaussians form is essentially a radial-basis function interpolant; it is known that such a representation has a universal approximation property [38] when all parameters are learnt appropriately.) The cost function for the minimisation exercise was computed as follows. Given a candidate parameter set/vector $\underline{a}$, the corresponding estimated source function $\hat{s}(t, \underline{a})$ was computed. This function was then used within the LISA code as the imposed force at the actuation point in order to predict the estimated response at the appropriate sensor point $\hat{r}(t, \underline{a})$. The cost function was then computed as the mean-square error between the estimated response $\hat{r}_i$ (sampled at times t_i) and the measured response from the test programme r_i.

$$J(\underline{a}) = \sum_{i=1}^{M} w_i(\hat{r}_i(\underline{a}) - r_i)^2 \tag{4}$$

where M is the number of response points measured, and w_i is a weighting function. The weighting function was used for the following reason. The response comprised a very small amplitude S_0 component followed by a substantial A_0 component which decreased in frequency and increased in amplitude as time progressed. In order that the initial high-frequency low-amplitude component of the antisymmetric mode was allowed to influence the optimisation, the response functions were multiplied by an exponentially decaying window. The window function was established on the basis of trial and error and its exact functional form was considered unimportant; the idea was not to optimise the window but just to increase the influence of the S_0 wave. Figure 2 shows the form of the window used, superimposed on the weighted response function.

The standard Differential Evolution (DE) algorithm of reference [39] was used to carry out the actual optimisation; this attempts to transform a randomly generated initial population of parameter vectors into an optimal solution through repeated cycles of evolutionary operations, in this case: *mutation*, *crossover* and *selection*. To assess the value of a given solution, a cost/fitness function is needed; the weighted mean-square error (WMSE) of equation (4) was used here. The following sequence of operations is carried out with each vector in the current population taken as a *target vector*; each of these vectors has an associated cost (WMSE). Each target vector is pitted against a *trial vector* in a competition which results in the vector with highest fitness or lowest cost advancing to the next generation.

The mutation procedure in basic DE runs is as follows; two vectors A and B are randomly chosen from the current population to form a vector differential $A - B$. A *mutated* vector is

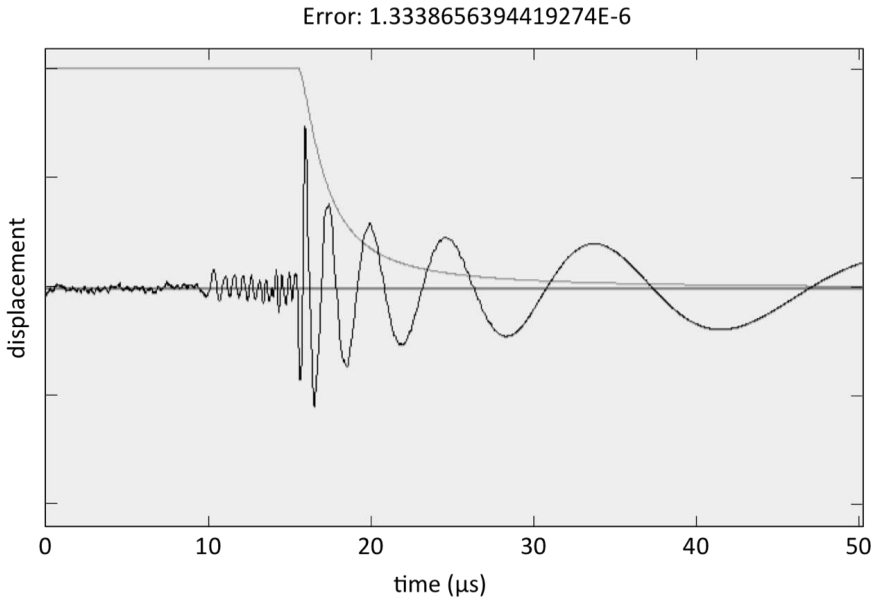

Figure 2: Weighting function for cost function superimposed on weighted wave response

then obtained by adding this differential, multiplied by a scaling factor F, to a further randomly chosen vector C to give the overall expression for the mutated vector: $C+F(A-B)$. The scaling factor, F, is often found have an optimal value between 0.4 and 1.0 [39].

A *trial vector* is then formed as the child of two vectors: the target vector and the mutated vector. It is obtained via a *crossover* process; in this work, uniform crossover was used. Uniform crossover decides which of the two parent vectors contributes to each chromosome of the trial vector by a series of $D-1$ binomial experiments, where D is the dimension of the parameter vectors. Each experiment is mediated by a crossover parameter C_r (where $0 \leq C_r \leq 1$). If a random number generated from the uniform distribution on [0,1] is greater than C_r, the trial vector takes its parameter from the target vector, otherwise the parameter comes from the mutated vector.

This process of evolving through the generations is repeated until the population becomes dominated by only a few high fitness or low cost solutions, any of which would be suitable. Like the vast majority of optimisation algorithms, convergence to the global maximum is not guaranteed; however, one of the benefits of the evolutionary approach, because it is population-based is that it is more resistant to finding a local maximum. Again, like most nonlinear optimisation algorithms, DE is sensitive to the initial conditions specified for its search. The user specifies a range for each parameter, and the initial population is formed by uniformly random sampling from the ranges. If a parameter leaves the allowed range as a result of evolutionary optimisations, it is pinned to the edge of the range for that individual. In the absence of prior knowledge, the initial ranges can be specified by carrying out a few short optimisation runs and adjusting the ranges until no parameters are pinned to the endpoints. The F and C_r *hyperparameters* also affect the results of DE. In terms of F, it was set at 0.8 as previous experience had shown this value working well in a range of problems; although this is a little large, it allows more movement in the search space in the initial stages of the process and therefore enhances the resistance to local minima. The crossover ration was chosen as 0.5 here; this means that a parameter in the trial vector is equally likely to come from either parent vector. Because the DE algorithm has a stochastic nature, ten or more runs were made on each data set and the parameters corresponding to the lowest cost (WMSE) were recorded each time. In the first case study, a population of 60 individuals was used and the algorithm was allowed to run for 500 generations.

4 Results: Case Study 1

As discussed early, the first case study was based on laser actuation, with response waveforms recorded at 6.3cm, 7.3cm and 8.3cm from the actuation point. The optimisation exercise was

carried out using the waveform data recorded 6.3cm from the actuation point in order to establish the cost function. As discussed above, the DE algorithm has a stochastic nature which makes it potentially dependent on the randomly generated initial population. In order to avoid sensitivity to initial conditions, the algorithm was run ten times using a different initial population in each case; a population of 60 individuals was used and the algorithm was allowed to run for 500 generations. The parameters corresponding to the source function were extracted in each case. Figure 3 shows the comparison between the measured and estimated response functions for the first of the runs. Superimposed in the figure is the source function estimated from this run; the correspondence between predicted and measured waveforms is excellent.

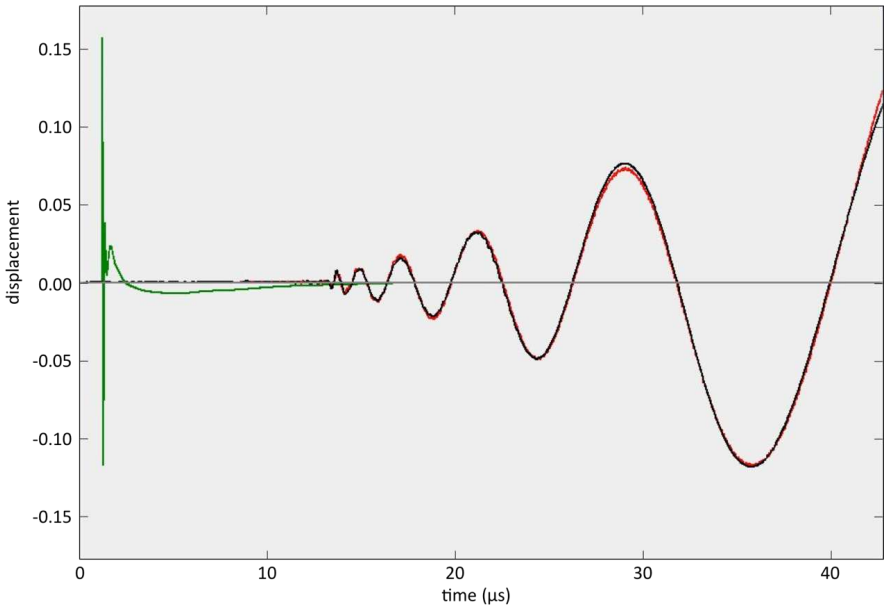

Figure 3: Results from the first run of the DE algorithm, the experimental results (black), the optimised impulse force (green - not to scale) and the simulated results for that impulse (red).

Convergence of the algorithm was quite rapid in terms of generations; the evolution of the best and average cost functions for the first run is shown in Figure 4. The values of the cost function for the ten runs are provided in Table 4. As the WMSE errors are not normalised, the absolute values of the errors do not carry much information (although one can gauge the size of the error function by noting that run 1 corresponds to the waveform comparison in Figure 3.) The best run gave a WMSE value of 1.3339×10^{-6} (the comparison is not shown because it is indistinguishable from that shown in Figure 3, which gave a WMSE value of 1.3384×10^{-6}). All ten identified source waveforms are shown in Figure 5.

Run Number	Cost function (fitness)$\times 10^6$
1	1.3384
2	1.9098
3	1.4118
4	1.3339
5	1.3779
6	1.4539
7	1.7190
8	1.3363
9	1.3537
10	1.3645

Table 1: Cost (fitness) values for the 13 runs of the DE algorithm.

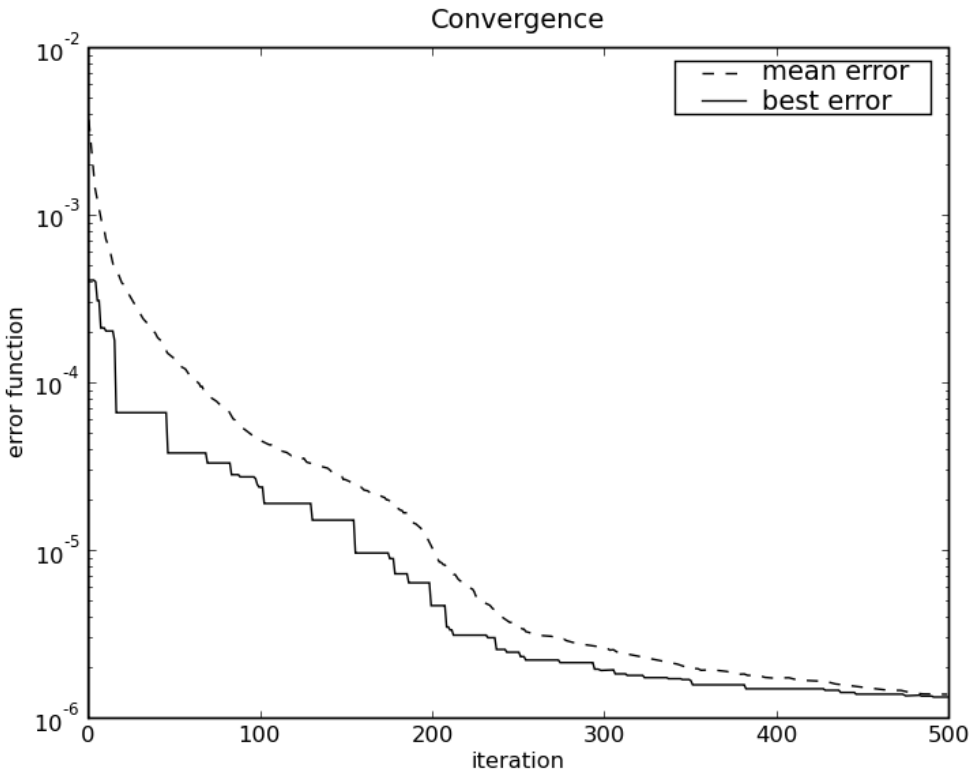

Figure 4: Convergence profile of DE algorithm on a single (the first) optimisation run.

An important question raised during this exercise related to the sensitivity of the simulation to the source function applied. As the determination of the source function is essentially an inverse problem (although it is implemented only using forward simulation runs here), there existed the possibility that a range of source functions could still yield a good correspondence between the measured and simulated responses, so the solution may not be unique. There are essentialy three pieces of evidence in support of the hypothesis that the procedure did in fact estimate the 'true' function. The first is based on engineering judgement: the lowest cost estimates of the source (as illustrated by Figure 3) do appear to agree with physical intuition; they are composed of an initial sharp transient corresponding to the ablative regime of the laser pulse [21], followed by a slower variation of low amplitude, consistent with the temperature variation induced by the localised heating from the pulse.

The second fact in support of the uniqueness of the solution is that the ten runs of the DE algorithm with different initial conditions all converged to very similar pulse waveforms, as shown by Figure 5. Most of the runs show the sharp initial transient with a consistent duration; however, some of the curves are qualitatively a little different; as mentioned above, the group with sharper initiation correspond to the solutions with lowest cost function, as illustrated in Figure 6.

The third, and strongest, piece of evidence in support of the estimated source function comes from *cross-validation*. In order to establish whether an estimated model has physical credibility, it must be tested on a different data set to the estimation data. In this study, cross-validation was carried out by comparing the response measured at 8.3cm with that predicted using the estimated source; the resulting comparison is shown in Figure 7; the agreement is excellent. The small phase error can potentially be explained by the fact that the source-response distance was measured with a steel rule which was only accurate to 1 mm, this means that there may well have been a small mismatch between the propagation distances in the actual plate and the LISA simulation. While this cross-validation lends considerable confidence to the predictive power of the algorithm, it is important to point out that the distance between the 6.3 cm and 8.3 cm response points is comparatively small; over larger distances, the dispersive nature of the

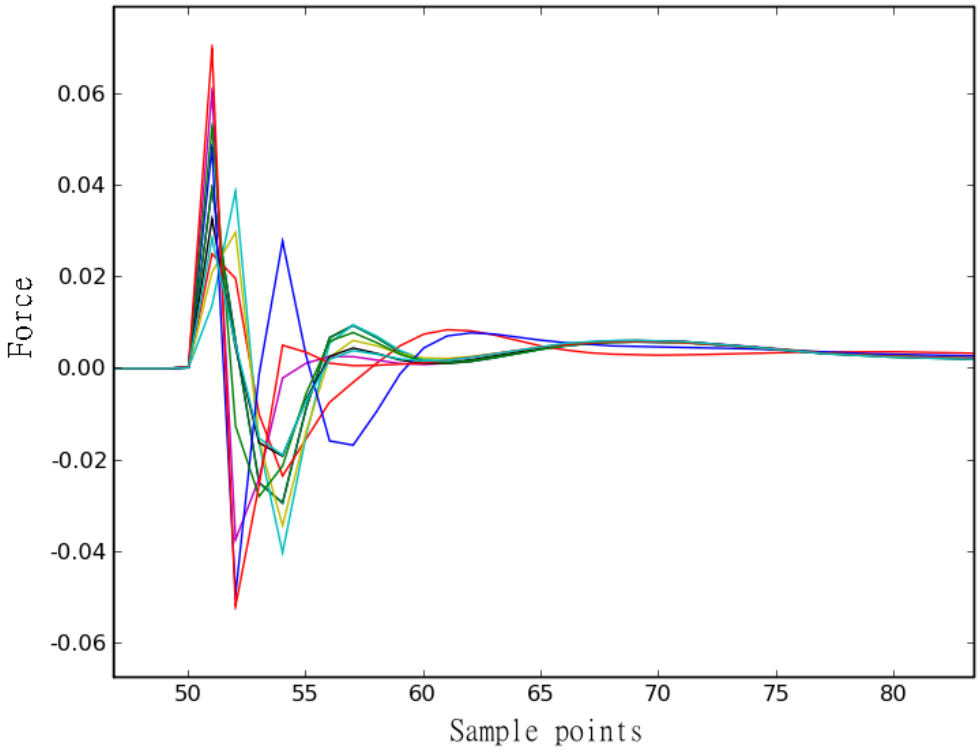

Figure 5: All ten source functions as estimated by the ten DE runs (The time scale is given in terms of sample points; to see the correspondence to physical units (μs), please consult Figure 6).

Lamb waves would be be more evident and would provide a more stringent test of the predictive capability of the algorithm. The later case studies did in fact collect data over a larger range of distances from the source.

5 Results: Case Study 2

The second case study moved to the more interesting (for SHM purposes) case of Hsu-Nielsen sources. Various data sets were recorded, but those analysed in this study were from three groups of pencil lead-breaks executed at distances 5mm, 50mm and 100mm from the laser vibrometer which was used to record the responses. Each group consisted of ten lead-breaks. The wave profiles were recorded from the vibrometer using an Infinium oscilloscope; 8192 points at 20 Msamples/s were recorded in each case. Figure 8 shows four of the responses recorded. The first trace (lead break no. 4) in Figure 8 corresponds to the data analysed later.

It is immediately clear from Figure 8 that the signal-to-noise for the lead-break responses was considerably lower than in the laser impulse case. In order to alleviate this problem, the responses were smoothed using a simple 31-point moving average with a uniform window; the results are shown in Figure 9. A further problem with the data emerged once the analysis began. In the experiments carried-out earlier with laser actuation, the oscilloscope was triggered using a photo-diode which responded to the source laser flash; this gave a reliable point of origin in time for the source. For the lead-break experiments, a standard threshold trigger was used on the scope and, because of the noise on the response, this introduced a degree of uncertainty in the initiation time of the source.

As before, the source function was represented by a sum of Gaussian functions, each being parametrised by its mean (centre in time) and standard deviation (extent in time). Because of the uncertainty associated with the oscilloscope triggering, another parameter was introduced to represent the onset time of the source. This parameter was bracketed by a trial and error

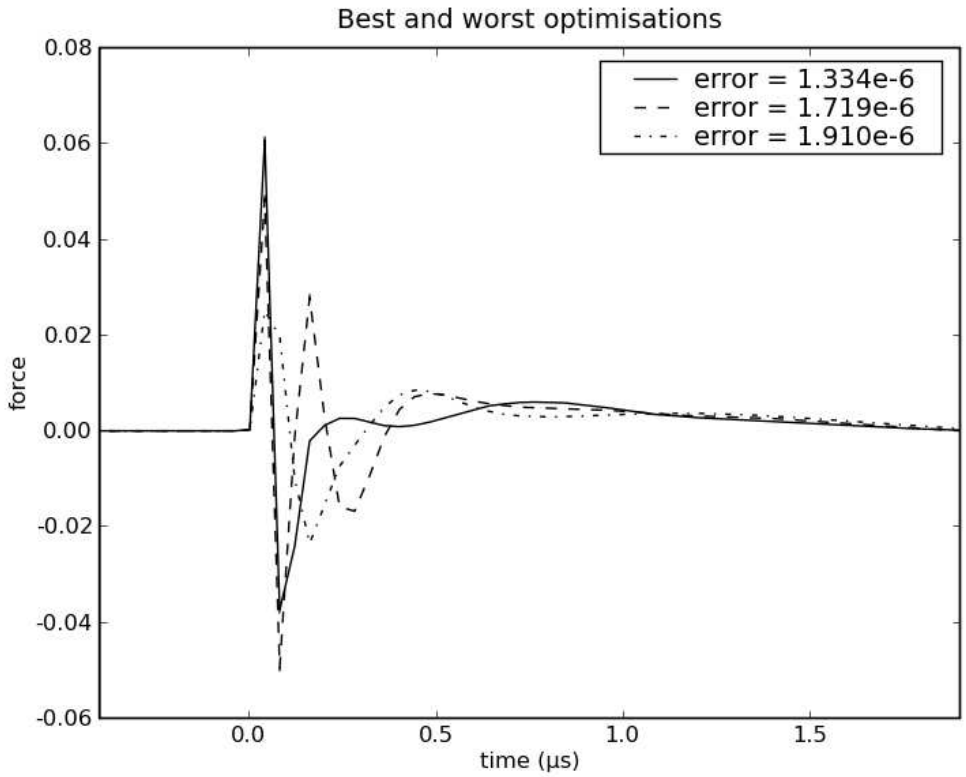

Figure 6: Best and (two) worst results from the optimisation in terms of the cost function values.

process of simulation where a series of trials indicated the bounds within which an onset could sensibly generate the recorded profiles; the trigger uncertainty placed another small demand on the analysis.

Another issue arose during the trial simulations. As indicated by equation (2), the LISA algorithm has an optimal time-step associated with the spatial cell size, an optimum associated with the stability of the solutions [10, 11]. If the time-step used is too high, instability of the algorithm results; if the step is too low, the predicted results may be sub-optimally accurate. In the simulations considered here, it was found that the 'optimal' time step for LISA was too long to allow accurate resolution of the high frequency component of the source. A time-step one-tenth the optimal size was used to solve this problem with the understanding that this might impact the accuracy of the response prediction. As before, a 2D implementation of the LISA algorithm was used and the objective/cost function for the DE optimisation was based on the WMSE between the measured and LISA-predicted responses as discussed. In this case study, the MSE was inverted to give a fitness function for maximisation.

As the first case study had been restricted to responses measured close the actuation point, it was considered interesting here to carry out the initial optimisation exercise using the waveform data recorded 100mm from the actuation point. As before, to avoid sensitivity to initial conditions in DE, the algorithm was run 13 times using a different initial population in each case. The fitness values achieved from the runs are given in Table 5. The parameters corresponding to the source function were extracted in each case. Figure 10 shows a comparison between the measured and estimated response functions for the best of the runs. The correspondence between predicted and measured waveforms is excellent and allays concern that the sub-optimal LISA time-step would have a negative impact on simulation accuracy.

All 13 of the estimated source functions from the DE runs are given in Figure 11; all are characterised by an initial sharp impulse followed by a peak of much longer duration; this matter will be discussed in more detail a little later.

Setting aside the issue of the longer-duration feature, Figure 12 singles out the initial sharp impulse of the optimised sources from the 13 DE runs; the best two in terms of fitness are

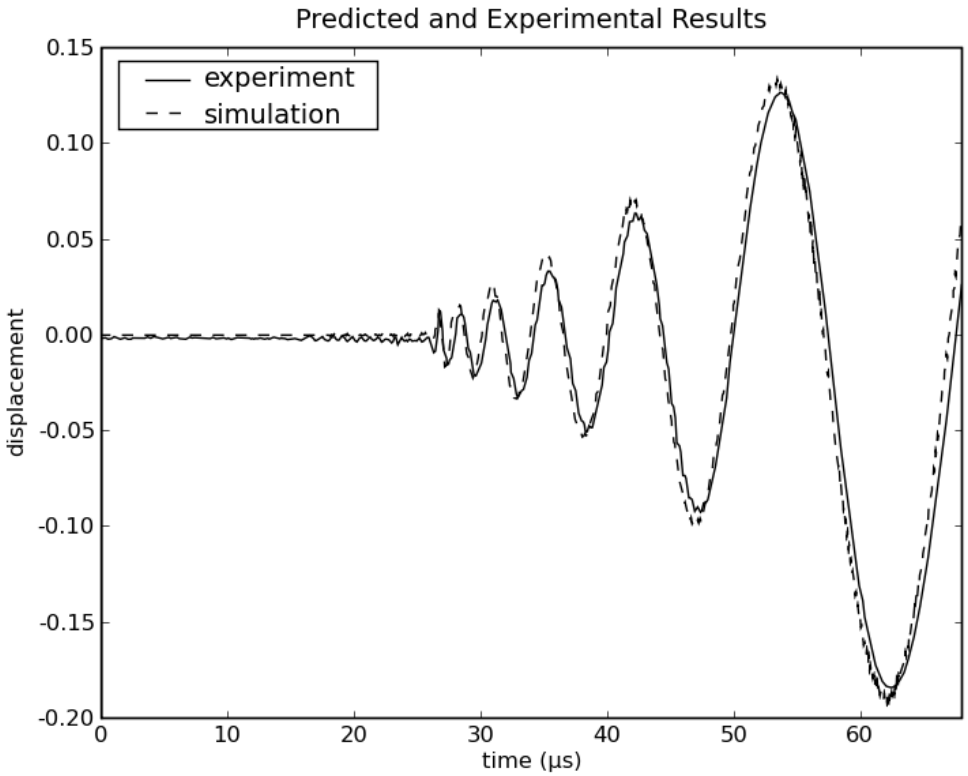

Figure 7: Best and (two) worst results from the optimisation in terms of the cost function values.

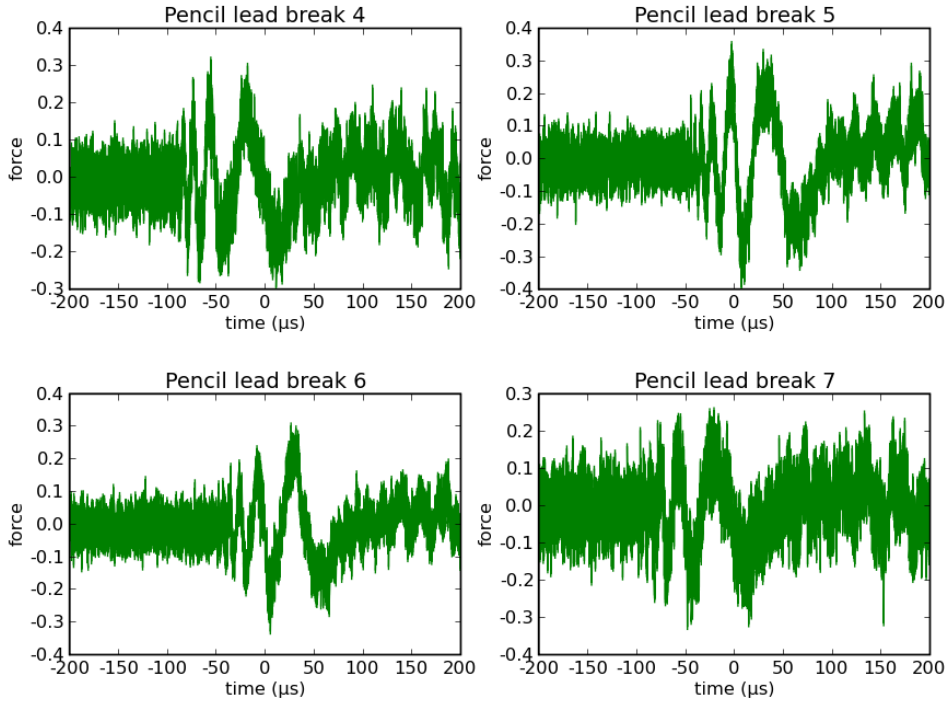

Figure 8: Four sample responses from pencil lead breaks at 100mm from the vibrometer spot.

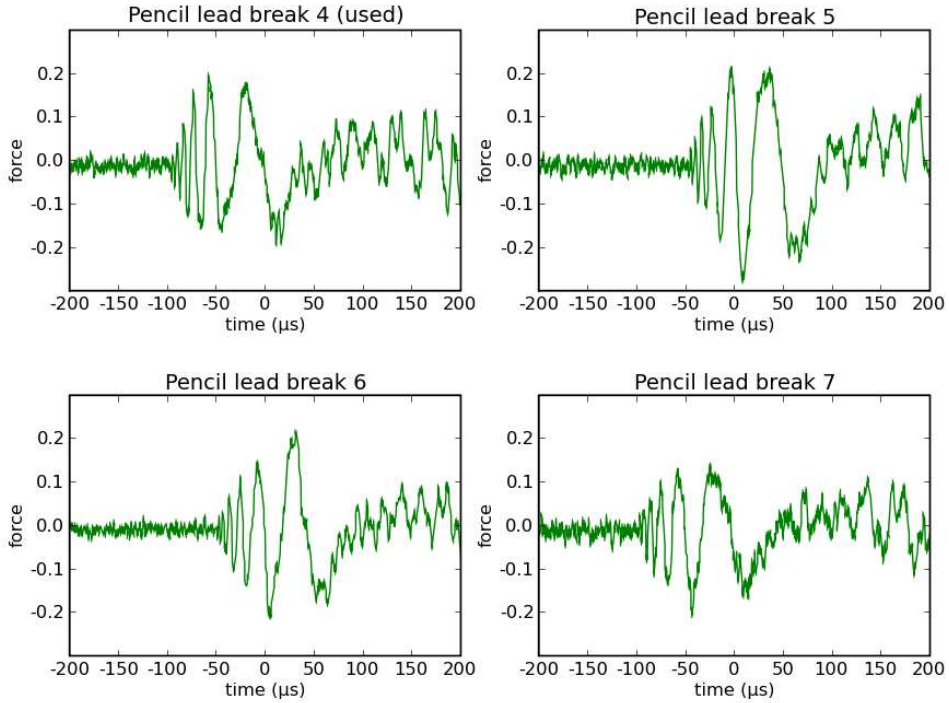

Figure 9: Smoothed responses corresponding to Fig. 2.

Run Number	Fitness (1/WMSE)
1	0.00453
2	0.00386
3	0.00353
4	0.00430
5	0.00440
6	0.00449
7	0.00437
8	0.00360
9	0.00453
10	0.00357
11	0.00446
12	0.00409
13	0.00374

Table 2: Cost (fitness) values for the 13 runs of the DE algorithm.

shown as solid lines in contrast to the remainder which are shown as dotted. It was considered encouraging that the best two solutions are in good agreement as to the onset time and shape of the initial sharp impulse.

It is necessary to return now to the issue of the longer-duration feature observed in all the estimated source functions. Unlike the laser-generated pulses considered earlier, in which longer-time behaviour could conceivable be associated with heating effects following the initial ablative impulse, there is no similar physical mechanism which comes immediately to mind in the case of the pencil lead breaks. One must consider other possible explanations. One of the first which springs to mind relates to the assumption of the 2D LISA simulation. As discussed previously, a difference between the 2D simulation and the 3D reality, arises because of geometrical attenuation. In fact, there is strictly no geometrical attention in the 2D simulation,

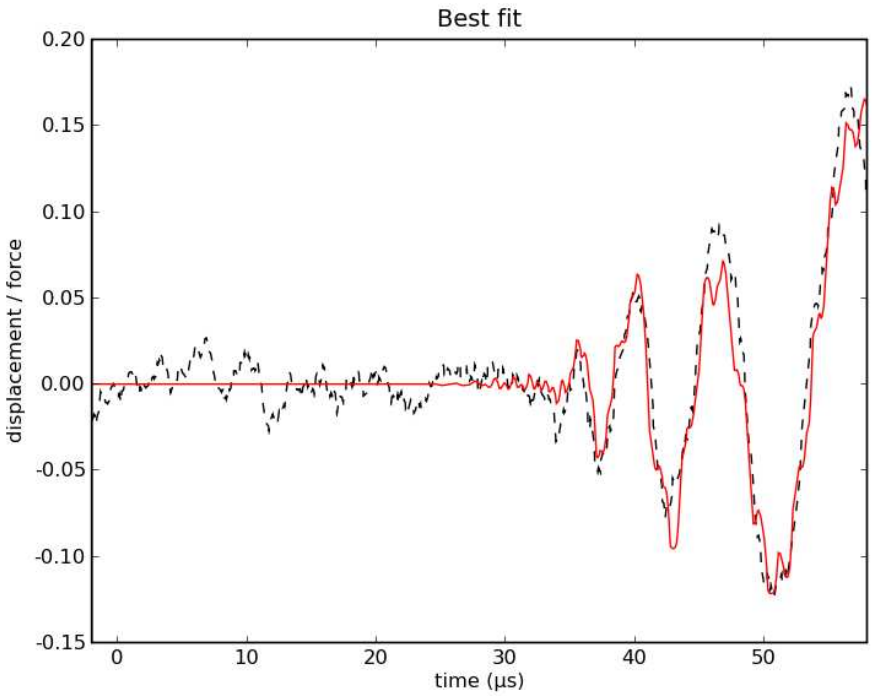

Figure 10: From the best run of the DE algorithm, the experimental results (dotted, black), and the simulated results for the optimal impulse (solid, red).

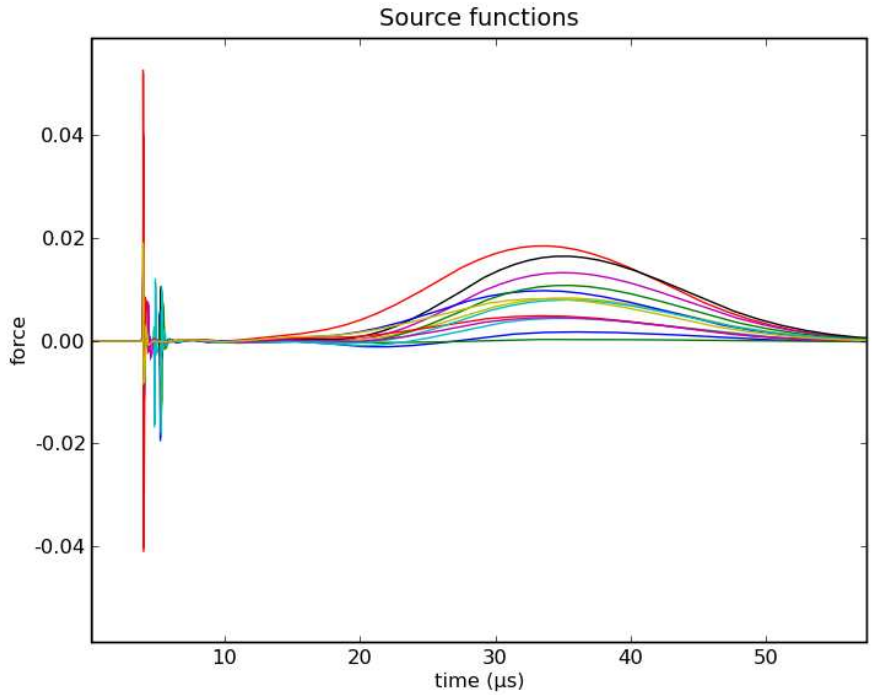

Figure 11: All 13 source functions as estimated by the DE runs.

as the wavefront does not spread out; the main source of attenuation (in the sense of decreasing amplitude with distance from the source) will come from dispersion. In contrast, the 3D reality will see marked geometrical attenuation. Although the wavefront energy would technically spread

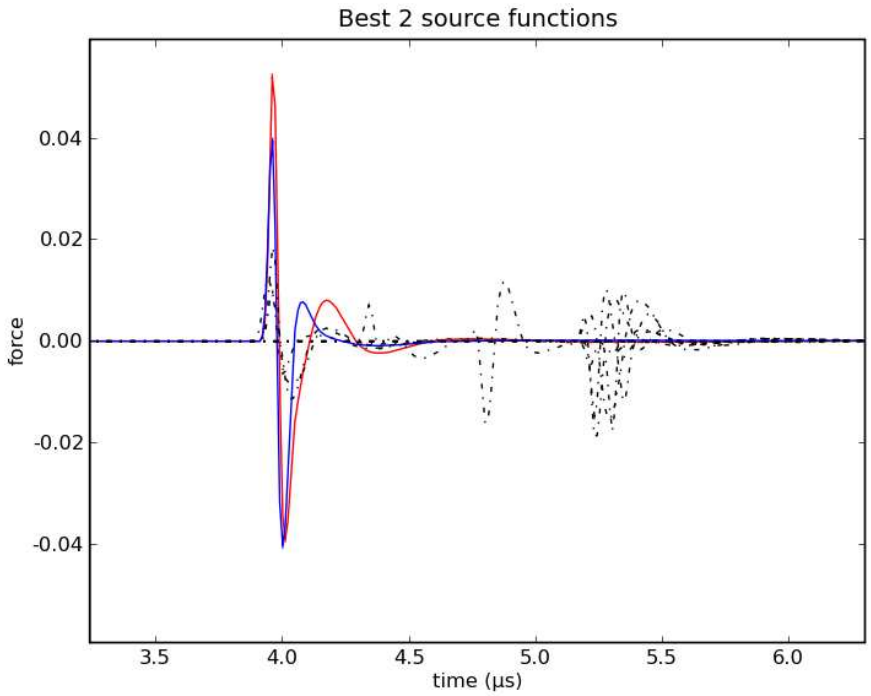

Figure 12: Initial segments of optimised source profiles from all 13 DE runs. Results with two best fitness results are shown as solid lines

out on the surface of a sphere, because of the confinement to the thin-plate, it is more realistic to think of it as spreading over an expanding circle. As the effect of this would be more visible at later times, it is plausible to see this as the origin of the longer-time source behaviour identified using the 2D LISA algorithm. In effect, 2D LISA is compensating for geometrical spreading by adding an extra feature to the estimated source. In order to investigate this hypothesis, a simulation was carried out with the best derived source function, but with the long-term component (it is associated with a single Gaussian in the expansion) removed. The resulting comparison between predicted and measured response is given in Figure 13.

As one might expect in the light of the preceding remarks, the simulation without the long-term feature in the impulse shows markedly greater growth of the waveform over the estimation window, suggesting that the long-term feature may well be accounting for the different physical mechanism of attenuation in the actual 3D data. Given this concern over the asymptotic behaviours of the 2D and 3D propagation models, it was considered necessary to pass directly to a 3D LISA simulation. At the time of the experiments, and for a period afterwards, it was not possible to implement the optimisation procedure wrapped around a 3D simulation. Fortunately, the coming of the CUDA implementation removed this problem and allowed the third case study. (Following the implementation of 3D LISA it was possible to revisit the issue of the long-term feature, and parallel 2D and 3D simulations did support the conclusions above.)

6 Results: Case Study 3

The third case study was concerned with the Hsu-Nielsen sources and built directly on the earlier work using the 2D LISA implementation. The optimisation methodology for source characterisation was applied as before, with the sole difference being that a 3D LISA simulation was allowed because a much faster implementation of the algorithm was coded using parallel processing on CUDA-enabled graphics processors. This software was developed by AGH University and EC Grupa in Krakow, Poland. The CUDA implementation brings the LISA algorithm back to its roots in a sense, as the original algorithm was conceived to run on a parallel computer (A *Connection Machine*).

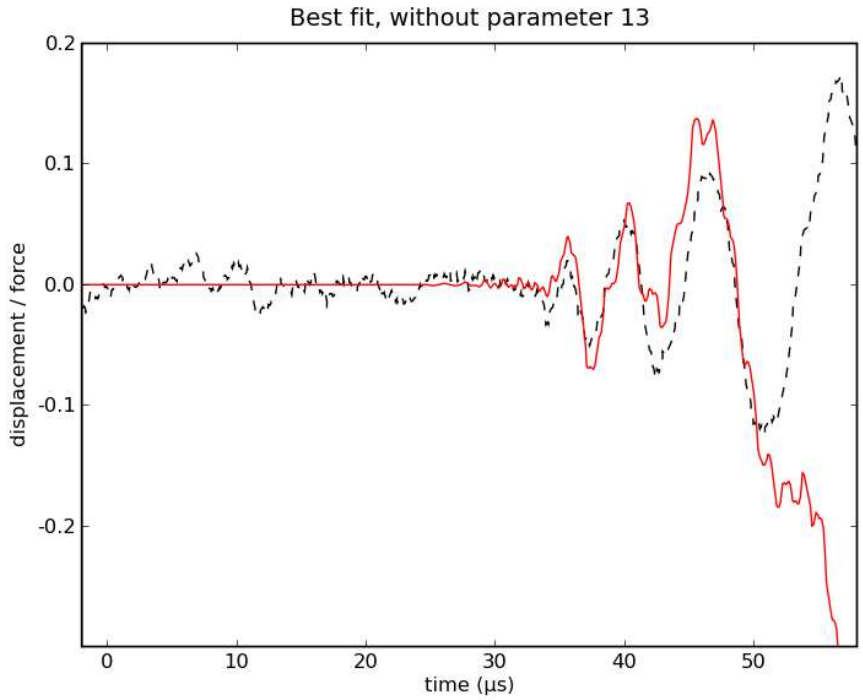

Figure 13: From the best run of the DE algorithm with the long-duration feature removed from the impulse: the experimental results (dotted, black), and the simulated results for the response (solid, red).

As in the 2D case, DE was used to characterise the source function. As before, multiple runs of the algorithm were carried out with different randomly-generated initial populations. The data for optimisation was taken from the lead-breaks carried out 5mm from the point of sensing for the vibrometer; ten lead-breaks were executed, and the resulting responses for all ten are shown in Figure 14[2]. In contrast, the responses for a validation set of ten lead-breaks at 50mm from the sensing point are shown in Figure 15. As there is essentially only one sensor (the laser vibrometer), it was not possible to measure the responses at different distances from the *same* source event; however, every attempt was made to apply the Hsu-Nielsen source in as repeatable a manner as possible. Many 'practice' breaks were carried out by the experimenters; furthermore, any 'double impact' events, caused by the lead guide contacting the plate following the break, were removed from the data.

One of the lead-break responses at 5mm (arbitrarily chosen as the 4^{th} in the set) was used for the DE optimisation. Only the first 32.5 μs of the response were used, in order to keep the time for each simulation low (Figure 16). Ten runs of DE were made with different random initial populations. The minimum costs (WMSEs) associated with each run are shown in Table 6.

The results from DE varied in cost from 0.00122 to 0.03163; all the identified impulses are shown in Figure 17. There is clearly some variation across the results; however, if the impulses from the four lowest costs are separated out, there is remarkable consistency (Figure 18).

The scatter in the response predictions from all ten identified impulses can be seen in Figure 19, superimposed on the experimental measurements. With the additional hindsight provided by the response predictions, it now appears that the impulses are grouped according to two separate minima, with the higher cost values associated with a local minimum.

Figure 20 shows the impulse response associated with the lowest cost compared to the mea-

[2]It is unfortunate, but the figures from this point onwards do not have vertical ticks or labels. This is not possible to fix because of changes in personnel on projects; the figures cannot be changed now without a complete re-analysis of the data, which is not currently possible. However, the lack of the scale is largely harmless as the main figures are provided as *comparisons* between source functions and responses. Furthermore, the reader is able to get some idea of scale from the figures included here for the second case study. Finally, although this is not an excuse for the oversight, one can argue that, as the LISA algorithm is linear, the overall scales are not significant.

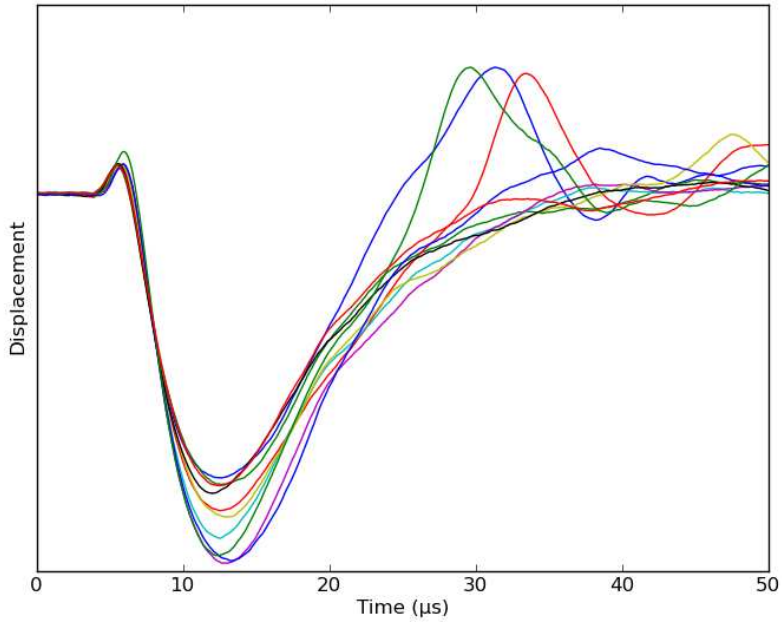

Figure 14: Experimental results for ten AE events (pencil lead breaks) showing measured displacement responses at 5mm from the sources.

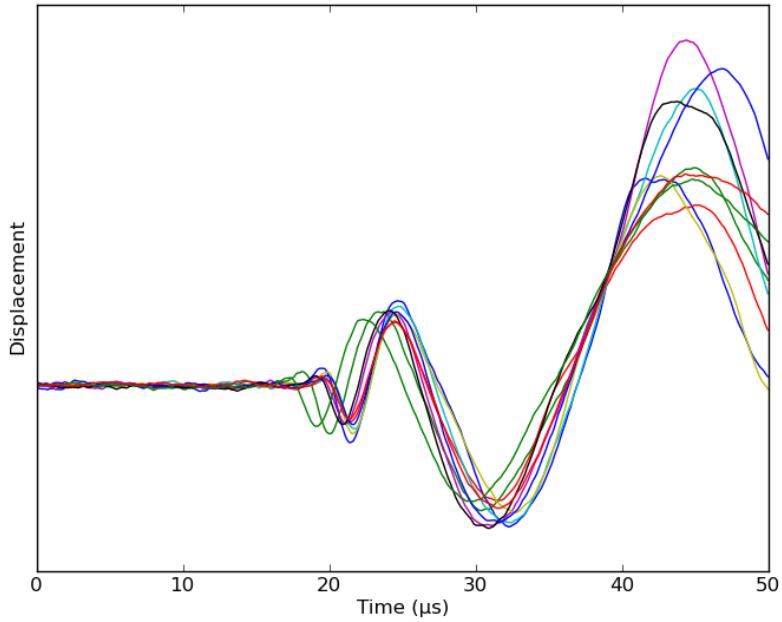

Figure 15: Experimental results for a different ten AE events (pencil lead breaks) showing displacement at 50mm from the source. These are aligned on the time dimension according to the oscilloscope trigger point (which can be seen to occur at about 40 μ s on this graph)

surements for the training data from 5mm; the results are clearly excellent. However, the final confirmation of the model must come from cross-validation on previously unseen measurements. With this in mind, the optimised source function was used in LISA to predict the responses at 50mm from the source, and the comparison with measurements is shown in Figure 21. Because

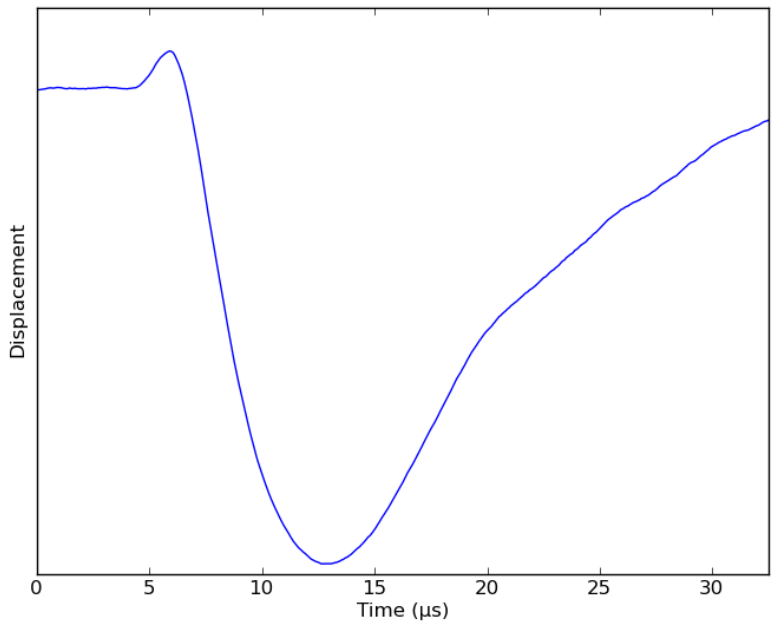

Figure 16: One of the experiments (No. 4) was taken as the basis for impulse optimisation. Only the first 32.5 μ s was used, to keep the time needed for each simulation low.

Run Number	Cost function (WMSE)
1	0.03163
2	0.03087
3	0.00372
4	0.00233
5	0.02942
6	0.00122
7	0.00651
8	0.03128
9	0.03123
10	0.00226

Table 3: Cost (fitness) values for the 10 runs of the DE algorithm.

it was not possible to show the actual response at 50mm corresponding to the training data, the predictions are shown together with the measured responses for all of the ten lead-breaks made 50mm from the sensor. The results appear to be excellent, the measured responses largely surround the prediction. Although there some discrepancies between 25 μs and 40 μs, the results appear to strongly support the optimisation methodology for source characterisation.

7 Discussion and Conclusions

There are two main conclusions to this paper; the first is that it has provided experimental validation for the 2D and 3D LISA algorithms in terms of prediction transient wave responses in thin-plate structures. The second conclusion, which emerged as the work progressed is potentially much more interesting. The results of the paper show that it is, in principle, possible to use an optimisation methodology in order to solve the problem of acoustic emission source characteristion. This conclusion is supported by the fact that a source function can be inferred

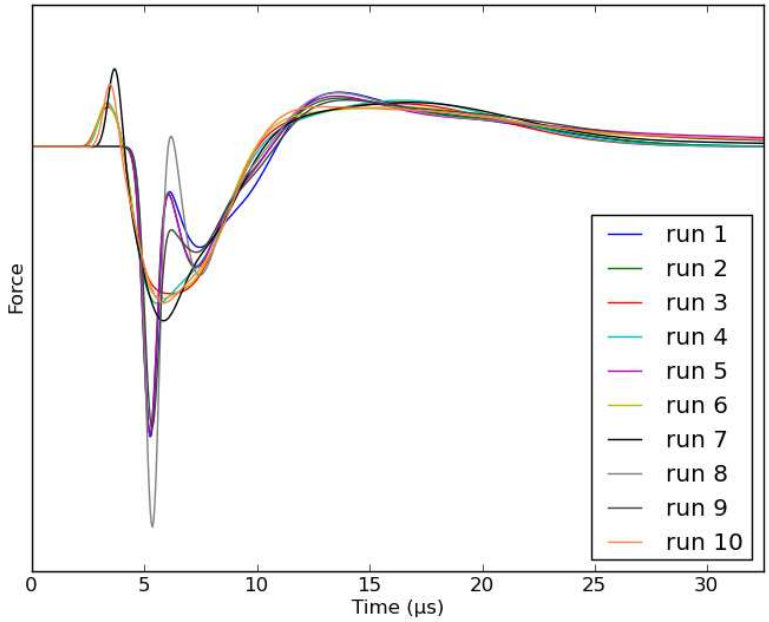

Figure 17: Impulses identified by each of the 10 runs.

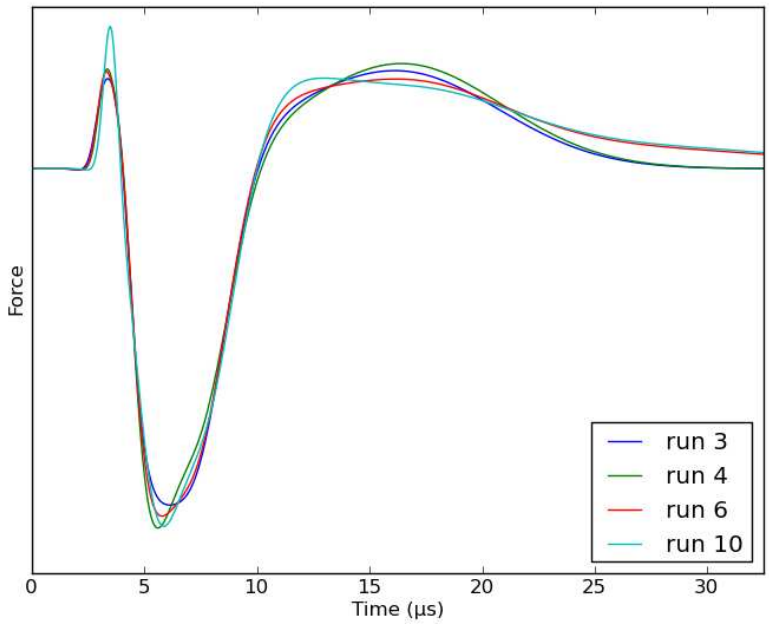

Figure 18: Impulses identified by the best 4 runs

which gives very good agreement with experimentally measured wave responses when used as the driving force for a numerical simulation. Further, it is established that the LISA algorithm provides a excellent basis for the wave simulation needed for the optimisation approach. The optimisation approach is successfully validated on both laser-generated ultrasound pulses and Hsu-Nielsen AE sources (pencil lead breaks). An accurate functional form for AE source functions can potentially be used in a number of useful ways in further work, not least in the analysis of uncertainty aspects of the source. Analysis of further pencil-lead breaks will allow

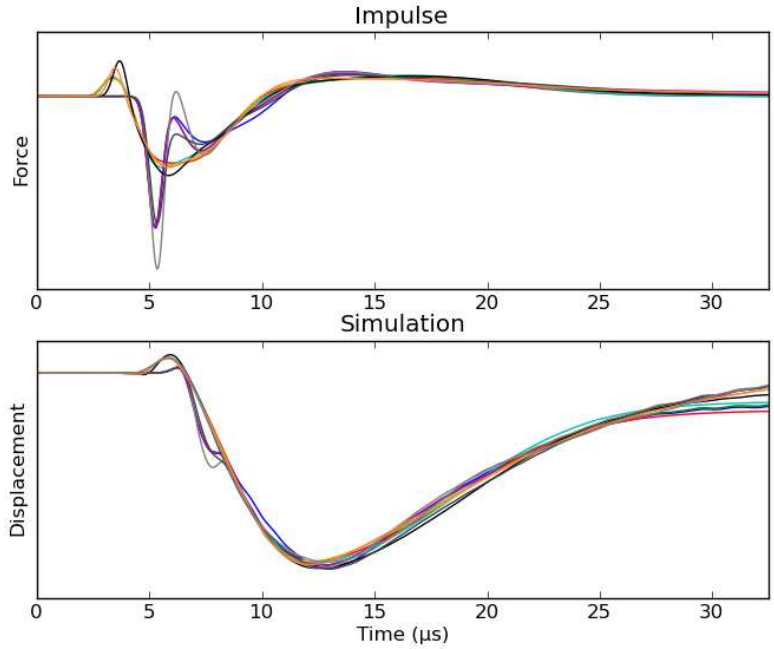

Figure 19: All 10 optimised impulses and the associated simulations for 5mm from source, together with the experimental result which was used for the optimisation.

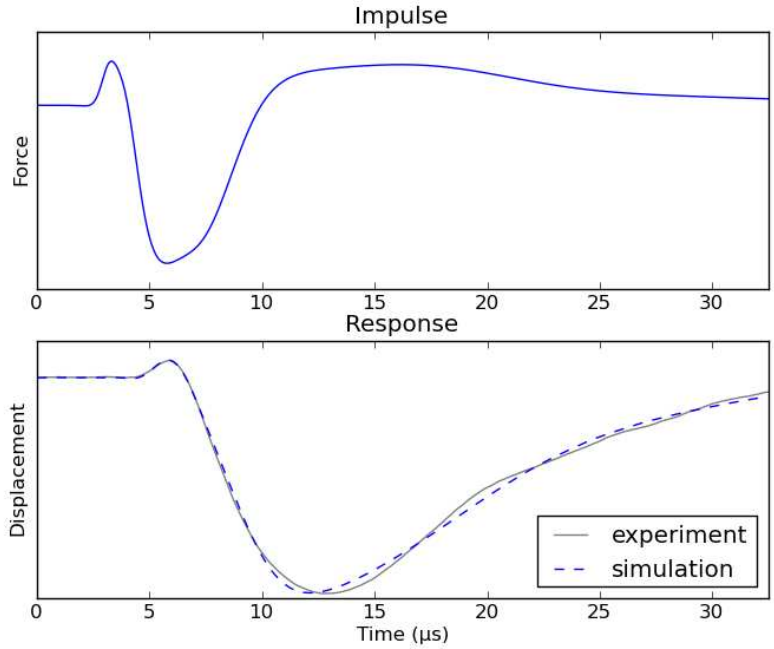

Figure 20: The best (least error) impulse and simulation for 5mm from source

a quantification of the source uncertainty in terms of ranges for the parameters of the adopted source function. This will allow one to bound the uncertainty on the wave responses; this is very useful information if one is to apply statistical interpretation techniques to measured responses as a means of achieving SHM. Also, from the SHM point of view, characterisation of the source function is likely to help if one is attempting to classify the source mechanism.

The results obtained here appear to be consistent in accuracy with papers cited in the Intro-

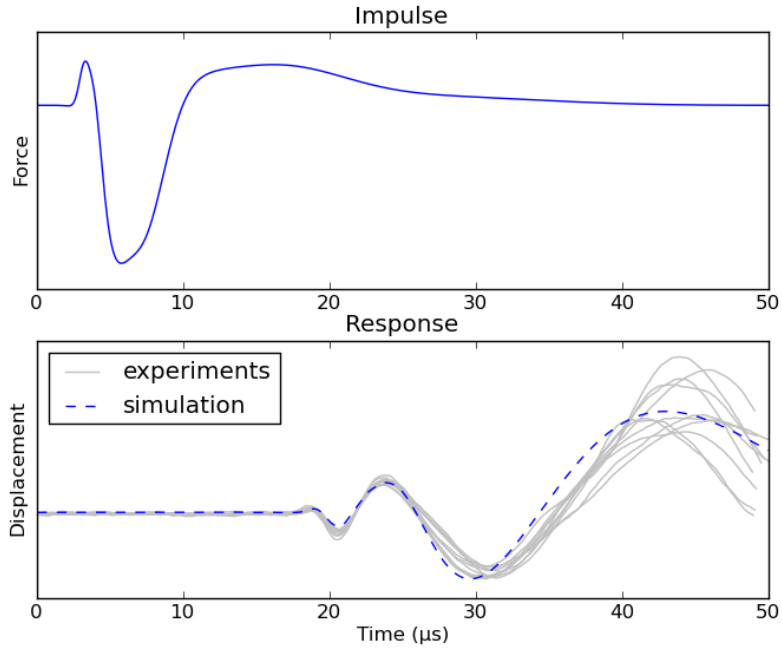

Figure 21: Best impulse and simulation at 50mm from source with the experimental results at 50mm

duction here. In particular the goodness of fit seen visually in Figure 21 is consistent with that shown in Figure 4 of [26], which also modelled AE wave propagation from pencil-lead breaks in aluminium plates. In that reference, the source is modelled as a linear ramp function with parameters informed by results obtained in [25, 40]. Comparison between identified source functions in given references is generally difficult as any sources identified will incorporate features of the experimental transduction/sensing hardware and associated instrumentation. In the current paper, the use of laser vibrometery has been used in order to minimise bandwidth and instrumentation issues, in order to expose more clearly the basic methodology. In fact, the methodology is generally applicable as long as the forward model adopted in the approach can actually model the transduction and instrumentation physics. As shown in [28], the relevant physics can be accommodated in an FE model; for the purposes of the current paper, the physics can also be captured in the LISA formulation – the commercial versions of the code used here [32, 33] allow modelling of piezoelectric transducers.

The work reported here has been carried out episodically over a number of years, but could still be considered preliminary in some senses. The main weakness of the work so far is perhaps the failure to completely adopt modern principles of machine learning. For example, the number of Gaussian basis functions in the fitted source function is actually a hyperparameter of the approach and should be determined in a principled manner, either by cross-validation or perhaps (adopting a Bayesian approach) by estimating model evidence. Another potential weakness is the trial-and-error setting of the delay parameters τ_i in the source function, although it is fair to say that the results presented here show that the pragmatic approach worked well. Adding the delay parameters would double the time taken for the DE optimisation, which is still quite long when 3D LISA simulations are used. One possibility would be to return to 2D simulations, but using the 2D LISA algorithm; this would now be very fast indeed with the CUDA system. However, there remains the problem of geometrical attenuation in the 2D algorithm. One option may be to carry out the wave simulation in a cylindrical polar coordinate system where a 2D form of the equations (independent of angle), would exactly reproduce the point source situation considered in this paper. This idea runs into problems because the wave equation is singular in cylindrical polars and so far has not produced useful results; however, work is continuing.

In terms of further work, one interesting problem for SHM purposes would be to characterise the source function for a propagating crack. This presents experimental difficulties in terms of

the fact that the source would be moving, and theoretical difficulties in terms of the fact that the physics is nonstationary. In general terms, one of the problems of applying the approach presented here will the need to account for the presence and physics of transducers; the issue was avoided here by using point actuation and sensing. New implementations of the CUDA version of LISA are already addressing this issue by handshaking of the LISA code with modelling software for piezoelectrics etc.

Acknowledgements

The authors would like to thank Dr Boon Lee, currently at Rolls-Royce, Derby, for providing a prototype of the 2D LISA code. This proved extremely useful in generating the current Java and CUDA implementations. They are also grateful to Dr Daley Chetwynd, also formerly of the Dynamics Research Group in Sheffield, for helping to track down and correct the mistakes in the LISA equations in the original publications.

References

[1] I. Viktorov. *Rayleigh and Lamb Waves: Physical Theory and Applications*. Plenum Press, 1970.

[2] J.L. Rose. *Ultrasonic Waves in Solid Media*. Cambridge University Press, 2004.

[3] D.N. Alleyne and P. Cawley. The interaction of Lamb waves with defects. *IEEE Transactions on Ultrasonics, Ferroelectrics and Frequency Control*, 39:381–397, 1992.

[4] A.J. Croxford, P.D. Wilcox, B.W. Drinkwater, and G. Konstantinidis. Strategies for guided-wave structural health monitoring. *Proceedings of the Royal Society A: Mathematical, Physical and Engineering Sciences*, 463:2961–2981, 2007.

[5] D.J. Buttle and C.B. Scruby. Characterization of fatigue of aluminum alloys by acoustic emission. I: identification of source mechanism. *Journal of Acoustic Emission*, ZZ:XX–YY, 1990.

[6] J.J. Hensman, R. Pullin, M. Eaton, K. Worden, K. Holford, and S.L. Evans. Detecting and identifying artificial acoustic emission signals in an industrial fatigue environment. *Measurement Science and Technology*, 20:045101, 2009.

[7] J.J. Hensman, R. Mills, S.G. Pierce, K. Worden, and M. Eaton. Locating acoustic emission sources in complex structures using gaussian processes. *Mechanical Systems and Signal Processing*, 24:211–223, 2010.

[8] J.J. Hensman, K. Worden, M. Eaton, R. Pullin, K. Holford, and S.L. Evans. Spatial scanning for anomaly detection in acoustic emission testing of an aerospace structure. *Mechanical Systems and Signal Processing*, 25:2462–2474, 2011.

[9] A. Balikin. Numerical simulation of guided waves for SHM - a literature survey. Technical report, Dynamics Research Group, Department of Mechanical Engineering, University of Sheffield, 2007.

[10] P.P. Delsanto, T. Whitcombe, H.H. Chaskelis, and R.B. Mignogna. Connection Machine simulation of ultrasonic wave propagation in materials. I - the one-dimensional case. *Wave Motion*, 16:65–80, 1992.

[11] P.P. Delsanto, R.S. Schecter, H.H. Chaskelis, R.B. Mignogna, and R. Kline. Connection Machine simulation of ultrasonic wave propagation in materials. II - the two-dimensional case. *Wave Motion*, 20:295–314, 1994.

[12] P.P. Delsanto, R.S. Schecter, and R.B. Mignogna. Connection Machine simulation of ultrasonic wave propagation in materials. III - the three-dimensional case. *Wave Motion*, 26:329–339, 1997.

[13] B.C. Lee and W.J. Staszewski. Lamb wave propagation modelling for damage detection. I: Two-dimensional analysis. *Smart Materials and Structures*, 16:249–259, 2007.

[14] B.C. Lee and W.J. Staszewski. Lamb wave propagation modelling for damage detection. II: Damage monitoring strategy. *Smart Materials and Structures*, 16:260–274, 2007.

[15] S.P. Rippengill, K. Worden, K.M. Holford, and R. Pullin. Automatic classification of ae data. *Strain*, 39:31–41, 2003.

[16] M.G.R. Sause, A. Gribov, A.R. Unwin, and S. Horn. Pattern recognition approach to identify natural clusters of acoustic emission signals. *Pattern Recognition Letters*, 33:17–23, 2012.

[17] N.N. Hsu and D.G. Eitzen. Acoustic emission source characterisation through direct time-domain deconvolution. In *Proceedings of the DARPA/AFML Review of Progress in Quantitative NDE, July 1978 - September 1979*, 1980.

[18] H.N.G. Wadley, C.B. Scruby, and G. Shrimpton. Quantitative acoustic emission source characterisation during low temperature cleavage and intergranular fracture. *Acta Metallica*, 29:399–414, 1980.

[19] T. Ohira, T. Kishi, H. Miyashita, Y. Kagawa, and E. Nakata. Transient behaviour of fibre fracture in tungsten/copper composites by means of acoustic emission source characterisation. *Transactions of the Japan Institute of Metals*, 27:484–495, 1986.

[20] C.B. Scruby. An introduction to acoustic emission. *Journal of Physics E: Scientific Instruments*, 20:20946, 1987.

[21] S.J. Davies, C. Edwards, G.S. Taylor, and S.B. Palmer. Laser-generated ultrasound: its properties, mechanisms and multifarious applications. *Journal of Physics D: Applied Physics*, 26:329–348, 1993.

[22] G. Manthei. Characterization of acoustic emission sources in a rock salt specimen under triaxial compression. *Bulletin of the Seismological Society of America*, 95:1674–1700, 2005.

[23] W.H. Prosser, M.A. Hamstad, J. Gary, and A. O'Gallagher. Finite element and plate theory modeling of acoustic emission waveforms. *Journal of Nondestructive Evaluation*, 18:83–90, 1999.

[24] M.A. Hamstad. Re-examination of NIST acoustic emission absolute sensor calibration: Part II: finite element modeling of acoustic emission signal from glass capillary fracture. *Journal of Acoustic Emission*, 29:175–183, 2011.

[25] M.G.R. Sause. Investigation of pencil-lead breaks as acoustic emission sources. *Journal of Acoustic Emission*, 29:184–196, 2011.

[26] M.G.R. Sause, M.A. Hamstad, and S. Horn. Finite element modeling of Lamb wave propagation in anisotropic hybrid materials. *Composites: Part B*, 53:249–257, 2013.

[27] J. Gary and M.A. Hamstad. On the far-field structure of waves generated by a pencil lead break on a thin plate. *Journal of Acoustic Emission*, 12:157–170, 1994.

[28] M.G.R. Sause and S. Richler. Finite element modelling of cracks as acoustic emission sources. *Journal of Nondestructive Evaluation*, 34:13, 2015.

[29] J.C̃uadra aand P.A.Ṽanniamparambil, D. Servansky, I. Bartoli, and A. Kontsos. Acoustic emission source modeling using a data-driven approach. *Journal of Sound and Vibration*, 341:222–236, 2015.

[30] N.N. Hsu. Acoustic emissions simulator, 1977. US Patent 4,018,084.

[31] T. Bielak, P. Paćko, A. Spencer, W.J. Staszewski, T. Uhl, and K. Worden. Cuda technology for lamb wave simulations. In *Proceedings of SPIE Conference, San Diego*, 2011.

[32] P. Paćko, T. Bielak, A.B. Spencer, W.J. Staszewski, T. Uhl, and K. Worden. Lamb wave propagation modelling and simulation using parallel processing architecture and graphical cards. *Smart Materials and Structures*, 21:075001, 2012.

[33] P. Paćko, T. Bielak, A.B. Spencer, T. Uhl, W.J. Staszewski, K. Worden, T. Barszcz, P. Russek, and K. Wiatr. Numerical simulations of elastic wave propagation using graphical processing units – comparative study of high-performance computing capabilities. *Computer Methods in Advanced Mechanical Engineering*, 290:98–126, 2015.

[34] S.G. Pierce, F. Dong, K. Atherton, B. Culshaw, G. Manson, K. Worden, T. Monnier, P. Guy, J.-C. Baboux, J. Assad, E. Moulin, S. Grondel, C. Delebarre, V. Agostini, P.-P. Delsanto, I. Genesio, E. Mino, and C. Boller. Damage assessment in smart composite structures: the damascos programme. In *Proceedings of SPIE Conference on Smart Materials and Structures, Newport Beach*, volume 4327, pages 223–233, 2001.

[35] A.C. Eringen and E.S. Suhubi. *Elastodynamics*, volume one. Academic Press, 1974.

[36] A.B. Spencer, K. Worden, W.J. Staszewski, J.A. Rongong, and N.D. Sims. An optimisation scheme based on the Local Interaction Simulation Approach and Lamb waves for elastic property estimation in multi-layered composites. *Shock and Vibration*, 19:1027–1040, 2012.

[37] G. Dobie, A.B. Spencer, K. Burnham, S.G. Pierce, K. Worden, W. Galbraith, and G. Hayward. Simulation of ultrasonic Lamb wave generation, propagation and detection for a reconfigurable air-coupled scanner. *Ultrasonics*, 51:258–269, 2011.

[38] C.M. Bishop. *Neural Networks for Pattern Recognition*. Oxford University Press, 1998.

[39] R. Storn and K. Price. Differential evolution–a simple and efficient heuristic for global optimization over continuous spaces. *Journal of global optimization*, 11(4):341–359, 1997.

[40] M.G.R. Sause, M.A. Hamstad, and S. Horn. Finite element modeling of conical acoustic emission sensors and corresponding experiments. *Sensors and Actuators: A Physical*, 184:64–71, 2012.